IAC-14-C1.1.7

SOLAR SAIL PERIODIC ORBITS IN THE EARTH-MOON THREE-BODY PROBLEM

Jeannette Heiligers
Advanced Space Concepts Laboratory, University of Strathclyde, United Kingdom, jeannette.heiligers@strath.ac.uk

Sander Hiddink
Delft University of Technology, the Netherlands, s.hiddink@student.tudelft.nl

Ron Noomen
Delft University of Technology, the Netherlands, r.noomen@tudelft.nl

Colin R. McInnes
Advanced Space Concepts Laboratory, University of Strathclyde, United Kingdom, colin.mcinnes@strath.ac.uk

Solar sailing has been proposed for a range of novel space applications, including hovering above the ecliptic for high-latitude observations of the Earth and monitoring the Sun from a sub-L_1 position for space weather forecasting. These applications, and many others, are all defined in the Sun-Earth three-body problem, while little research has been conducted to investigate the potential of solar sailing in the Earth-Moon three-body problem. This paper therefore aims to find solar sail periodic orbits in the Earth-Moon three-body problem, in particular Lagrange point orbits. By introducing a solar sail acceleration to the Earth-Moon three-body problem, the system becomes non-autonomous and constraints on the orbital period need to be imposed. In this paper, the problem is solved as a two-point boundary value problem together with a continuation approach: starting from a natural Lagrange point orbit. the solar sail acceleration is gradually increased and the result for the previous sail performance is used as an initial guess for a slightly better sail performance. Two in-plane steering laws are considered for the sail, one where the attitude of the sail is fixed in the synodic reference frame (perpendicular to the Earth-Moon line) and one where the sail always faces the Sun. The results of the paper include novel families of solar sail Lyapunov and Halo orbits around the Earth-Moon L_1 and L_2 Lagrange points, respectively, for both solar sail steering laws. These orbits are double-revolution orbits that wind around or are off-set with respect to the natural Lagrange point orbit. Finally, the effect of an out-of-plane solar sail acceleration component and the Sun-sail configuration is investigated, giving rise to additional families of solar sail periodic orbits in the Earth-Moon three-body problem.

I. INTRODUCTION

Solar sail technology is rapidly gaining momentum after recent successes such as JAXA's IKAROS mission [1] and NASA's NanoSail-D2 mission [2]. Research in the field is flourishing and new solar sail initiatives are scheduled for the future, including NASA's Sunjammer mission [3] (launch post-2015) and The Planetary Society's LightSail-1 mission [4] (launch 2016). Additional proposals include NASA's Lunar Flashlight and NEA Scout [5] missions.

The potential of solar sailing lies in the fact that, contrary to other low-thrust propulsion technologies like electric propulsion, solar sailing does not rely on an on-board propellant source. By exploiting the radiation pressure generated by solar photons reflecting off a large, highly reflective membrane, solar sails can produce a continuous thrust force that is only limited by the lifetime of the membrane material in the space environment. They therefore enable long-lived and high-energy mission concepts that have abundant novel applications [6].

One dynamical system commonly used to describe the motion of the solar sail is the Sun-Earth circular restricted three-body problem (CR3BP). This well-known system yields five natural equilibrium solutions (the L_1 to L_5 Lagrange points). Adding a propulsive thrust force, such as generated by a solar sail, to this CR3BP complements these five Lagrange points with an infinite set of artificial equilibrium points (AEPs). The literature proposes the use of these AEPs to hover over the poles of the Sun for heliophysics [7] or to hover along the Sun-Earth line for space weather forecasting [3]. In addition, periodic orbits around these AEPs have been suggested for further space weather monitoring capabilities [8] and parking a spacecraft above the orbit of the Earth for high-latitude observations, navigation and communication [9].

A dynamical system less investigated for solar sailing is the Earth-Moon CR3BP, the most likely reason being that the system is non-autonomous: as the Sun can be considered to rotate around the Earth-Moon system once per synodic lunar month, the direction of the photons impinging on the solar sail changes accordingly. As a result, AEPs in the Earth-Moon problem are only stationary instantaneously: their coordinates are time-dependent and either control is

required to compensate for the moving Sun-line or the sail has to navigate along the time-changing AEPs [10]. Finding solar sail periodic orbits in the Earth-Moon system adds another complexity in that the period of the orbit has to be equal to a fraction (or multiple) of the synodic lunar month in order for the orbit to be periodic.

Previous work on solar sail periodic orbits in the Earth-Moon system either linearised the equations of motion [11, 12] or searched for bespoke orbits (e.g. below the lunar South Pole [13]) by solving the optimal control problem. This work will instead look for entire families of solar sail periodic orbits, in particular Lyapunov and Halo orbits, in the Earth-Moon system by solving the accompanying boundary value problem. The existence of such families, closer to Earth than possible in the Sun-Earth system, can potentially give rise to unrivalled Earth observation capabilities or lunar far-side communication capabilities.

The structure of the paper is as follows. First, the non-autonomous dynamical system is described in Section II, followed by a definition of the two-point boundary value problem (BVP) to be solved in Section III. Section IV subsequently describes the initial guess and continuation scheme used to solve the two-point BVP for increasing solar sail performances. Then, after describing the adopted in-plane solar sail steering laws in Section V, the results are presented in Sections VI and VII for solar sail Lyapunov orbits at the L_1-point and solar sail Halo orbits at the L_2-point, respectively. Then, in Section VIII further constraints on the solar sail steering law are investigated, while Section IX considers an out-of-plane solar sail acceleration component. Finally, the effect of the Sun-sail configuration at time $t=0$ (i.e. the choice for the initial condition) is investigated in Section X and the paper ends with the conclusions.

II. DYNAMICAL SYSTEM

In the circular restricted three-body problem (CR3BP), the motion of an infinitely small mass, m, (i.e. the solar sail spacecraft), is described under the influence of the gravitational attraction of two much larger primary masses, m_1 (the Earth) and m_2 (the Moon). The gravitational influence of the small mass on the larger masses is neglected and the larger masses are assumed to move in circular orbits about their common center-of-mass.

Figure 1 shows the reference frame that is employed in the CR3BP: the origin coincides with the center-of-mass of the system, the x-axis connects the larger masses and points in the direction of the smaller of the two, m_2, while the z-axis is directed perpendicular to the plane in which the two larger masses move. The y-axis completes the right handed reference frame. Finally, the frame rotates at constant angular velocity, ω, about the z-axis, $\boldsymbol{\omega}=\omega\hat{\mathbf{z}}$.

New units are introduced (see also Table 1): the sum of the two larger masses is taken as the unit of mass, i.e. $m_1+m_2=1$. Then, with the mass ratio $\mu=m_2/(m_1+m_2)$, the masses of the large bodies become $m_1=1-\mu$ and $m_2=\mu$. As unit of length, the distance between the main bodies is selected, and $1/\omega$ is chosen as unit of time yielding $\omega=1$, and so one lunar month is represented by 2π. The conversion factors to change between dimensional and non-dimensional masses, distances and time are given in Table 1.

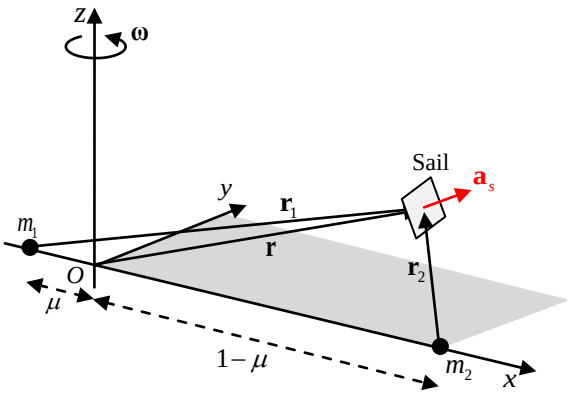

Figure 1 Schematic of CR3BP

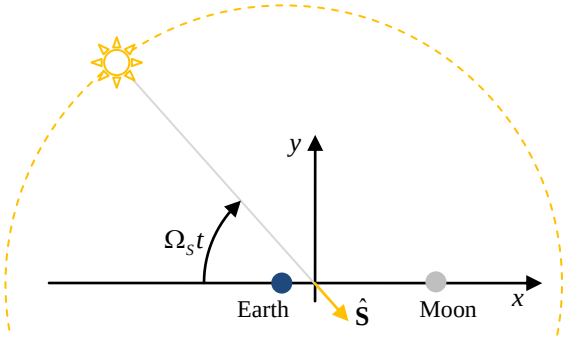

Figure 2 Schematic of non-autonomous Earth-Moon three-body problem

	Earth-Moon CR3BP
μ	0.01215
Total mass (m_1+m_2)	6.04718×10^{24} kg
Earth-Moon distance	384,401 km
One time unit	3.7749×10^{5} s
Ω_S	0.9252

Table 1 Earth-Moon CR3BP parameters

In this reference system, the motion of the solar sail is described by: [6]

$$\ddot{\mathbf{r}} + 2\boldsymbol{\omega}\times\dot{\mathbf{r}} + \boldsymbol{\omega}\times\left(\boldsymbol{\omega}\times\mathbf{r}\right) = \mathbf{a}_s - \nabla V \tag{1}$$

with $\mathbf{r} = \begin{bmatrix} x & y & z \end{bmatrix}^T$ the position vector of m. The terms on the left hand side are the kinematic, coriolis and centripetal accelerations, respectively, while the terms on the right hand side are the solar sail acceleration and the gravitational acceleration exerted by the primary masses. The gravitational potential, V, is given by:

$$V = -\left(\frac{1-\mu}{r_1} + \frac{\mu}{r_2}\right) \tag{2}$$

with the vectors $\mathbf{r}_1$ and $\mathbf{r}_2$ defined as $\mathbf{r}_1 = \begin{bmatrix} x+\mu & y & z \end{bmatrix}^T$ and $\mathbf{r}_2 = \begin{bmatrix} x-(1-\mu) & y & z \end{bmatrix}^T$. Following Reference [6], the centripetal acceleration in Eq. (1) can be written as the gradient of a scalar potential function, $\Phi = -\frac{1}{2}\left\|\boldsymbol{\omega}\times\mathbf{r}\right\|^2$, and can be combined with the gravitational potential into a new, effective potential, U:

$$U = -\frac{x^2+y^2}{2} - \left(\frac{1-\mu}{r_1} + \frac{\mu}{r_2}\right) \tag{3}$$

The new set of equations of motion then becomes:

$$\ddot{\mathbf{r}} + 2\boldsymbol{\omega}\times\dot{\mathbf{r}} = \mathbf{a}_s - \nabla U \tag{4}$$

Finally, for the solar sail acceleration, an ideal sail model is assumed [6]. An ideal solar sail is a sail that is perfectly reflecting. The incoming solar photons are therefore specularly reflected and the solar radiation pressure force acts perpendicular to the sail surface, in direction $\hat{\mathbf{n}}$. Furthermore assuming that the solar radiation pressure is constant in magnitude throughout the Earth-Moon system, the solar sail acceleration, $\mathbf{a}_s$, can be written as:

$$\mathbf{a}_s = a_{0,EM}\left(\hat{\mathbf{S}}\cdot\hat{\mathbf{n}}\right)^2\hat{\mathbf{n}} \tag{5}$$

In Eq. (5), $\hat{\mathbf{S}}$ is the direction of the Sun-line, see Figure 2, which can be expressed as:

$$\hat{\mathbf{S}} = \begin{bmatrix} \cos(\Omega_S t) & -\sin(\Omega_S t) & 0 \end{bmatrix}^T \tag{6}$$

with Ω_S the angular rate of the Sun-line in non-dimensional units, see also Table 1. Note that Eq. (6) ignores the small inclination difference between the Sun-Earth and Earth-Moon orbital planes and at time $t = 0$, the Sun is assumed to be on the negative x-axis.

Finally, note that $a_{0,EM}$ is the sail's characteristic acceleration in non-dimensional units. The characteristic acceleration is the acceleration generated by the solar sail when it faces the Sun at Earth's distance (at 1 Astronomical Unit). Derived from the Sunjammer sail performance, a typical characteristic is 0.215 mm/s^2 [14], which translates into a value for $a_{0,EM}$ of 0.0798.

III. BOUNDARY VALUE PROBLEM

Due to the non-autonomous behaviour of the system, periodic orbits are found by treating the problem as a two-point boundary value problem (BVP) rather than using conventional methods such as differential correctors [15]. The dynamics of the BVP are given in Eq. (4) and the boundary constraints are given by:

$$\mathbf{x}(t_0) = \mathbf{x}(t_f) \tag{7}$$

with $\mathbf{x} = \begin{bmatrix} \mathbf{r} & \dot{\mathbf{r}} \end{bmatrix}^T$, the indices '0' and '$f$' indicating the initial and final conditions and $t_f = 2\pi/\Omega_S$, i.e. one synodic lunar month.

The BVP is solved using the collocation method implemented in the MATLAB® *bvp4c.m* function.

IV. INITIAL GUESS

To solve the two-point boundary value problem, *bvp4c.m* needs an initial guess. Here, a continuation approach is adopted, where the search for solar sail periodic orbits starts from a natural periodic orbit with a suitable period. The sail performance in terms of characteristic acceleration $a_{0,EM}$ is then slowly increased and the solution for the previous value for $a_{0,EM}$ is used as initial guess for the next value for $a_{0,EM}$. This will in the end give rise to families of periodic orbits for increasing value of the sail performance.

IV.I Lyapunov orbit around L_1

The selection of the initial, natural Lyapunov orbit around the L_1 Lagrange point is shown in Figure 3a. These natural Lyapunov orbits are generated using the approach described in Reference [15] and their orbital periods are provided in Figure 3b. Only the Lyapunov orbits with a period equal to a fraction of the synodic lunar month would be suitable initial guess candidates, i.e. the following constraint applies:

$$P_{\text{Nat Lyap}} = \frac{1}{i}\frac{2\pi}{\Omega_S} \text{ with } i = 1,2,3... \tag{8}$$

The orbit that fulfils this constraint is indicated with a thick blue line in plot a) and with a blue asterisk in plot b). The selected Lyapunov orbit has a period of $P_{\text{Nat Lyap}} = \frac{1}{2}\frac{2\pi}{\Omega_S}$ and thus makes two orbital revolutions in one synodic lunar month.

a)

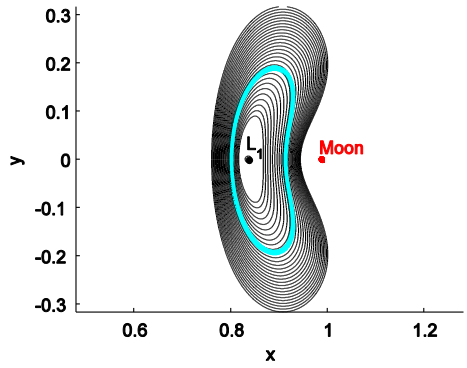

b)

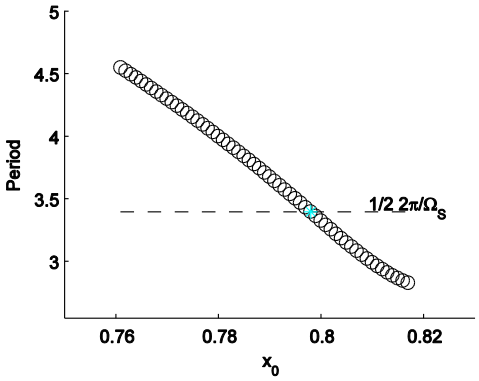

Figure 3 Lyapunov family at L_1. a) Lyapunov orbits. b) Period of Lyapunov orbits in a).

a)

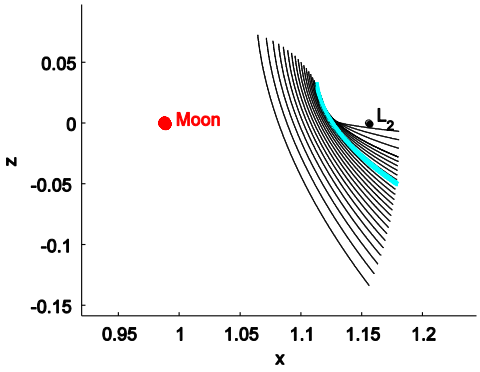

b)

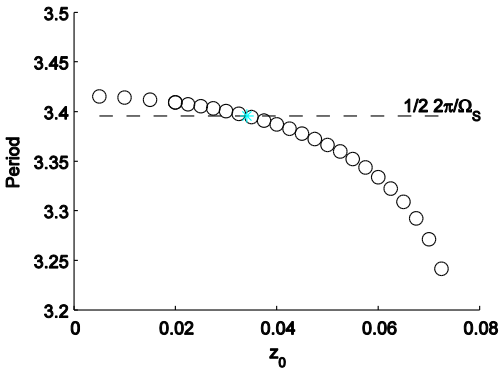

Figure 4 Northern Halo family at L_2. a) Halo orbits. b) Period of Halo orbits in a).

IV.II Halo orbit around L_2

The approach to find the initial, natural Halo orbit around the L_2 Lagrange point is very similar to the approach described for the Lyapunov orbit around L_1. The family of natural (northern) Halo orbits around L_2 is provided in Figure 4a with their orbital periods in Figure 4b. Again, the orbit with a period equal to a fraction of the synodic lunar month is chosen as suitable initial guess, which in this case also has a period of $P_{\text{Nat Halo}} = \frac{1}{2}\frac{2\pi}{\Omega_S}$ and therefore makes two orbital revolutions in one synodic lunar month.

V. SOLAR SAIL STEERING LAWS

Different families of solar sail periodic orbits can be generated for different solar sail steering laws. The two laws investigated in this paper are:

1) The sail normal is always directed along the Earth-Moon line, i.e. along the x-axis:

$$\hat{\mathbf{n}} = \text{sign}\left(\cos\left(\Omega_S\right)\right)\begin{bmatrix}1 & 0 & 0\end{bmatrix}^T \tag{9}$$

This steering law allows for a constant attitude of the sail in the CR3BP reference frame (and therefore a constant acceleration direction), but implies a changing solar sail acceleration magnitude. Note that the term $\text{sign}\left(\cos\left(\Omega_S\right)\right)$ takes into account that the solar sail acceleration changes sign when the Sun moves from a position where it illuminates the Earth-facing side of the sail to a position where it illuminates the Moon-facing side of the sail. Note that this implies that the solar sail has to be reflective on both sides. Since, conventionally, solar sail are only reflective on one side (to allow thermal emission on the rear side), Section VIII will consider the effects of constraining the steering law for a one-sided reflective solar sail.

2) The sail normal is always directed along the Sun-sail line, i.e. the sail always faces the Sun:

$$\hat{\mathbf{n}} = \hat{\mathbf{S}} \tag{10}$$

Contrary to the first steering law, this steering law allows for a constant magnitude of the sail acceleration ($\mathbf{a}_s = a_{0,EM}\hat{\mathbf{S}}$), but requires a changing attitude of the sail in the CR3BP reference frame.

VI. RESULTS – L_1 LYAPUNOV ORBITS

This section presents the families of solar sail Lyapunov orbits around the Earth-Moon L_1-point and for the two steering laws outlined in the previous section. The maximum solar sail characteristic acceleration considered is $a_{0,EM} = 0.088$, which is slightly larger than Sunjammer's performance, but indicates what could be feasible in the near-term.

VI.I Sail normal along Earth-Moon line

When assuming that the sail normal is always directed along the Earth-Moon line, the family of solar sail Lyapunov orbits as shown in Figure 5a can be obtained: the family originates from the natural Lyapunov orbit (see Figure 3) and is created by slowly increasing the characteristic acceleration, $a_{0,EM}$, of the solar sail. The larger the value for $a_{0,EM}$, the more the solar sail orbit deviates from the natural Lyapunov orbit.

The orbit for the largest characteristic acceleration, i.e. $a_{0,EM} = 0.088$, is provided in Figure 5b which clearly shows the difference between the natural and solar sail orbits: the solar sail Lyapunov orbit winds around the natural orbit and clearly makes two revolutions within one synodic lunar month. As the sail can only produce the maximum solar sail acceleration at time $t = 0$ and $t = \pi/\Omega_S$ (and generates no acceleration at $t = \pi/2\Omega_S$ and $t = 3\pi/2\Omega_S$), the offset between the natural and solar sail orbits is only small. Note that the asterisk indicates the initial condition of the orbit, which is chosen to be the y-axis crossing on the Earth-side of the L_1-point. Section X will investigate the influence of choosing a different initial condition on the shape of the solar sail periodic orbits.

VI.II Sail normal along Sun-sail line

The family of solar sail Lyapunov orbits around the L_1-point that can be generated by orienting the sail normal along the Sun-sail line is provided in Figure 6a. The change in orbit compared to the natural Lyapunov orbit is much greater than for the Earth-Moon line steering law in Figure 5 as the maximum sail acceleration can be exploited throughout the entire orbital period.

a)

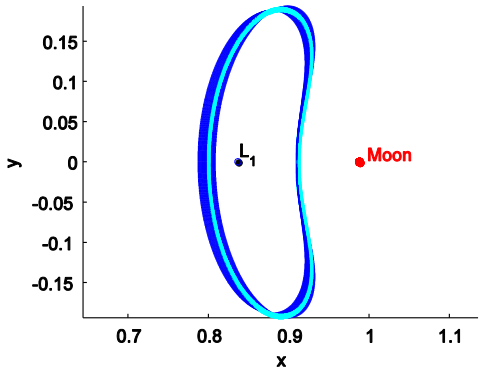

b)

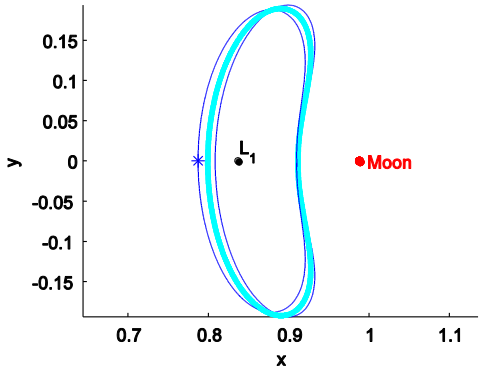

Figure 5 Solar sail Lyapunov orbits at L_1 with Earth-Moon line steering law. The thick cyan orbit is the natural Halo orbit in Figure 3a. a) Family of orbits. b) Orbit for $a_{0,EM} = 0.088$ (asterisk is initial condition)

a)

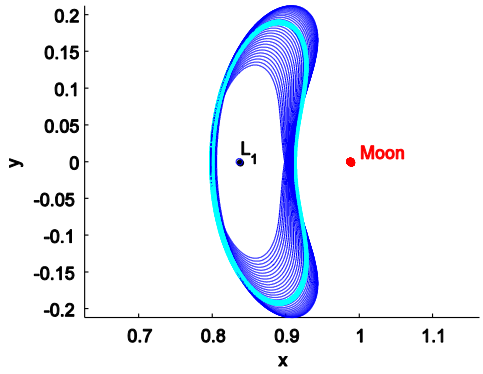

b)

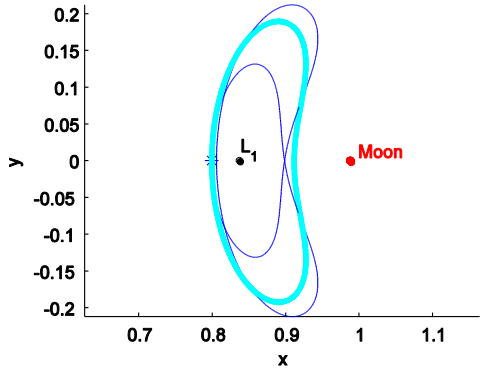

Figure 6 Solar sail Lyapunov orbits at L_1 with Sun-sail line steering law. The thick cyan orbit is the natural Lyapunov orbit in Figure 3a. a) Family of orbits. b) Orbit for $a_{0,EM} = 0.088$ (asterisk is initial condition).

The greater difference between the natural and solar sail orbit is also clear from Figure 6b that shows the solar sail Halo orbit for $a_{0,EM}$ = 0.088. This orbit clearly shows the two orbital revolutions per synodic lunar month with an inner and outer loop that are much smaller and greater than the natural Lyapunov orbit, respectively.

VII. RESULTS – L_2 HALO ORBITS

This section presents the families of solar sail Halo orbits around the L_2-point of the Earth-Moon system and for the two steering laws as outlined in Section V.

VII.I Sail normal along Earth-Moon line

When assuming that the sail normal is always directed along the Earth-Moon line, the family of solar sail Halo orbits as shown in Figure 7 can be obtained.

When comparing with the result for the Lyapunov orbits in Figure 5 (i.e. using the same solar sail steering law), a very similar effect of the solar sail acceleration on the in-plane motion can be observed: the solar sail periodic orbit winds around the natural periodic orbit. However, for the Halo orbits in Figure 7, the solar sail acceleration also affects the out-of-plane motion as it flattens the Halo orbit, positioning the southern part of the orbit closer to the Moon. From Figure 8, which shows the solar sail orbit for the largest characteristic acceleration considered, this is particularly clear. Again, the asterisk in plots c-d indicates the initial condition, which is chosen to be the y-axis crossing on the far-side of the L_2-point.

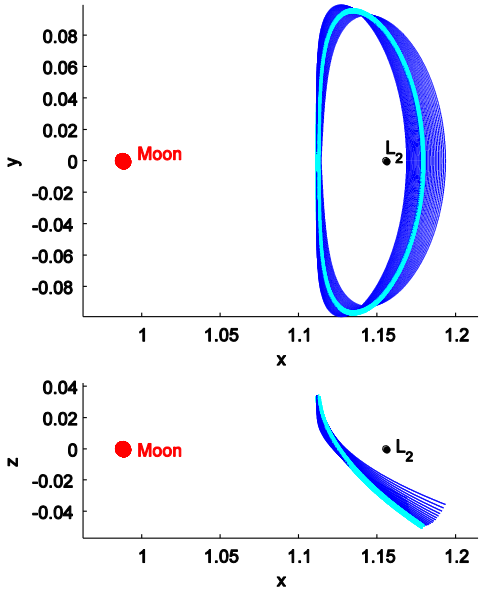

Figure 7 Family of solar sail Halo orbits at L_2 with Earth-Moon line steering law. The thick cyan orbit is the natural Halo orbit in Figure 4a.

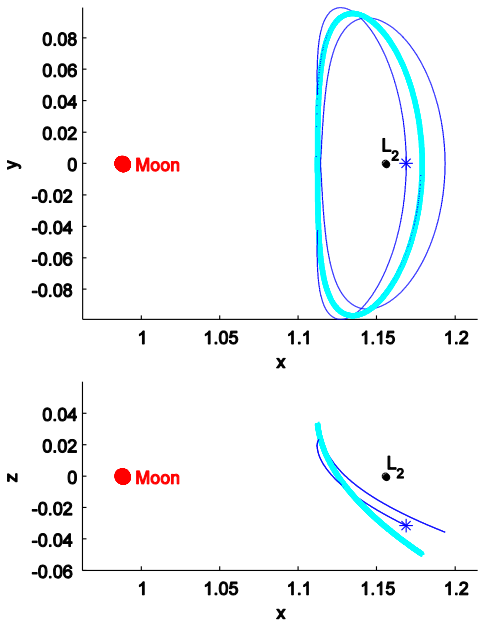

Figure 8 Solar sail Halo orbit at L_2 with Earth-Moon line steering law and $a_{0,EM}$ = 0.088. The thick cyan orbit is the natural Halo orbit in Figure 4a (asterisk is initial condition).

VII.II Sail normal along Sun-sail line

The final family to be considered is the solar sail Halo orbit family at the L_2-point with a Sun-sail line steering law. The results are presented in Figure 9, while Figure 10 provides the orbit for two characteristic accelerations, $a_{0,EM}$ = 0.044 (plots a-b) and $a_{0,EM}$ = 0.088 (plots c-d).

Figure 9 shows a very interesting result: by increasing the solar sail performance, the out-of-plane motion of the solar sail Halo orbit decreases until the Halo orbit reduces to a planar solar sail Lyapunov orbit. A similar effect can potentially be expected when further increasing the sail performance for the Earth-Moon line steering law in Section VII.I.

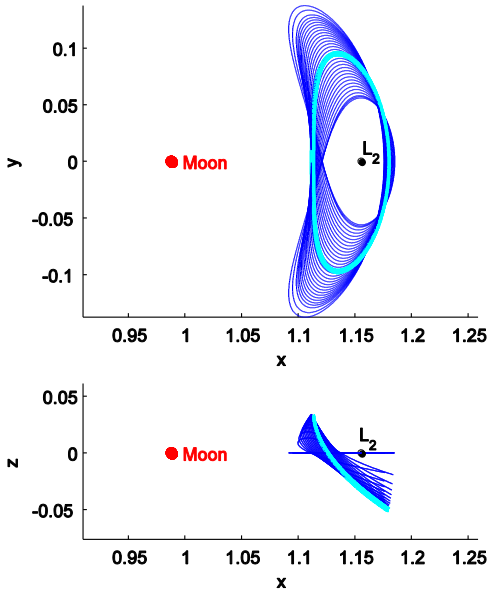

Figure 9 Family of solar sail Halo orbits at L_2 with Sun-sail line steering law. The thick cyan orbit is the natural Halo orbit in Figure 4a.

VIII. ONE-SIDED REFLECTIVE SOLAR SAIL

As mentioned in Section V, the solar sail steering law in Eq. (9) assumes that the solar sail is reflective on both sides. While this may be achievable in the long-term, a more near-term scenario would be that the solar sail is only reflective on one side, the front side (i.e. the Earth-facing side), and will have a highly thermally emitting rear surface. This is to emit the absorbed energy of the small fraction of incident solar radiation that, in reality, will be absorbed by the sail substrate [6]. The rear surface should therefore not be exposed to sunlight. To take this into account, this section imposes an additional constraint that 'switches the sail off' when the Sun illuminates the rear side of the sail:

$$\begin{aligned} \mathbf{a}_s &= a_{0,EM}\left(\hat{\mathbf{S}}\cdot\hat{\mathbf{n}}\right)^2\hat{\mathbf{n}} \quad \text{if } \left(\hat{\mathbf{S}}\cdot\hat{\mathbf{n}}\right)\geq 0 \\ \mathbf{a}_s &= \mathbf{0} \qquad\qquad\qquad\quad \text{if } \left(\hat{\mathbf{S}}\cdot\hat{\mathbf{n}}\right)< 0 \end{aligned} \tag{11}$$

Note that a zero acceleration can be achieved by positioning the sail edge-wise to the Sun-line. Also note that $\left(\hat{\mathbf{S}}\cdot\hat{\mathbf{n}}\right)=\cos\left(\Omega_S t\right)$ and therefore the constraint $\mathbf{a}_s=\mathbf{0}$ is imposed when $\frac{1}{2}\pi\leq t\leq\frac{3}{2}\pi$.

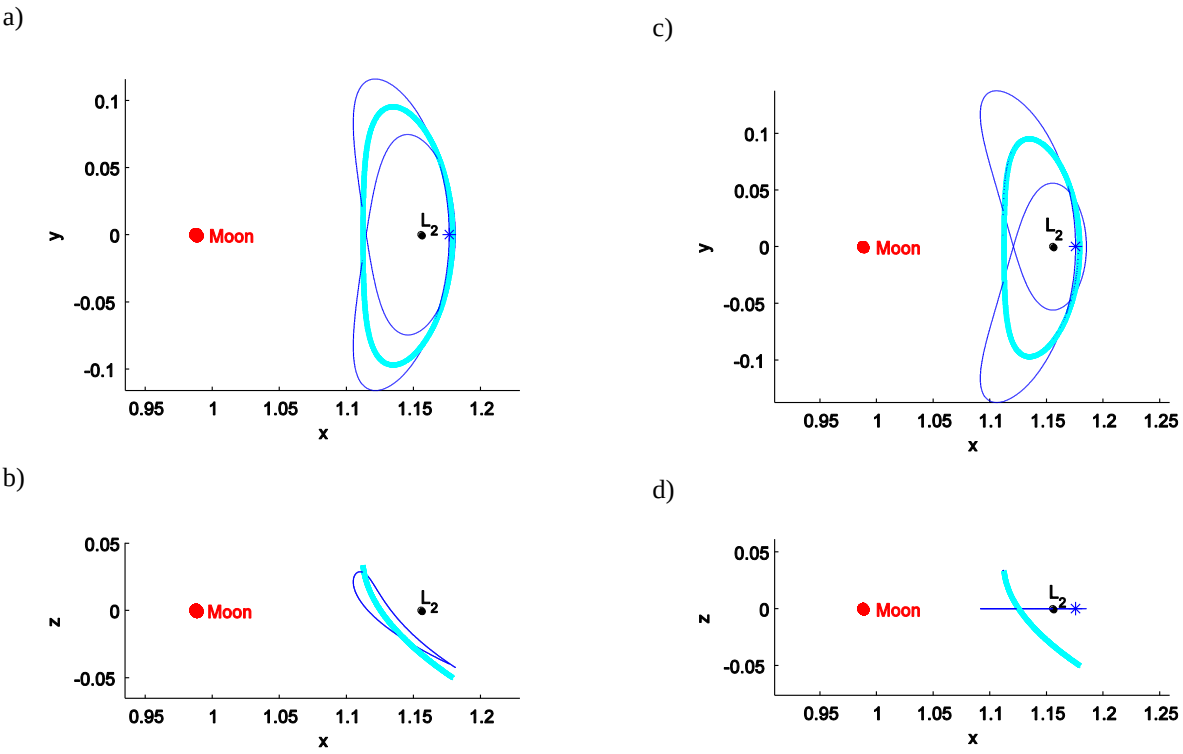

Figure 10 Solar sail Halo orbit at L_2 with Sun-sail line steering law. The thick cyan orbit is the natural Halo orbit in Figure 4a. The asterisks are the initial conditions. a) $a_{0,EM}$ = 0.044. a) $a_{0,EM}$ = 0.088.

The result is provided in Figure 11 and Figure 12 for the solar sail Lyapunov orbits at L_1 and the solar sail Halo orbits at L_2, respectively.

When considering the Lyapunov orbits, it becomes clear that exploiting the solar sail acceleration only when the Sun is on the Earth-side of the orbit results in very minor deviations from the natural Lyapunov orbit. However, it is clear that those parts of the orbit where the solar sail acceleration acts (i.e. the first half of the first revolution and the second half of the second revolution) are displaced towards the Sun.

Considering the solar sail Halo orbits with the constrained Earth-Moon line steering law, the solar sail acceleration has a much greater effect even though it only acts during half of the orbital period. In the out-of-plane direction a similar effect as for the orbits in Figure 9 can be observed, i.e. the out-of-plane motion decreases for increasing sail performances until the orbit reduces to a planar solar sail Lyapunov orbit.

a)

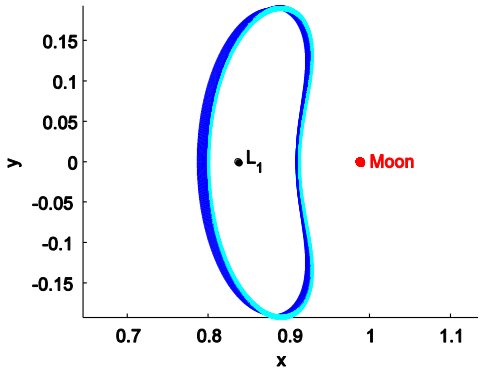

b)

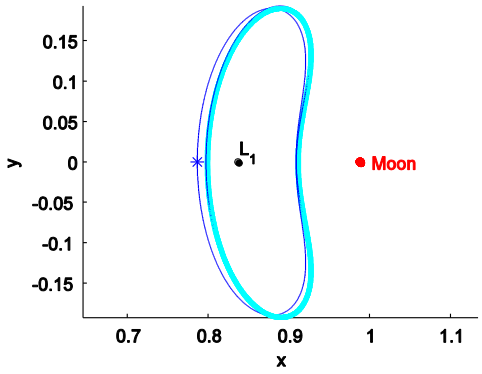

Figure 11 Solar sail Lyapunov orbits at L_1 with *constrained* Earth-Moon line steering law. The thick cyan orbit is the natural Halo orbit in Figure 3a. a) Family of orbits. b) Orbit for $a_{0,EM} = 0.088$ (asterisk is initial condition).

a)

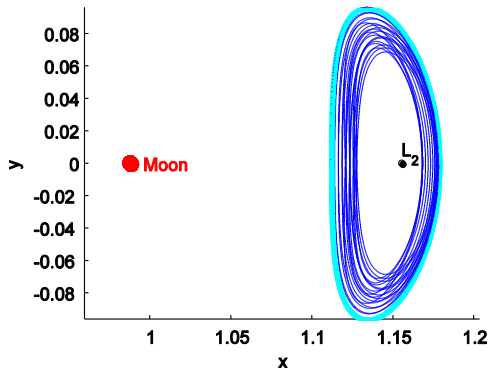

b)

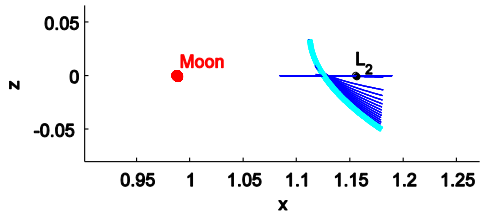

c)

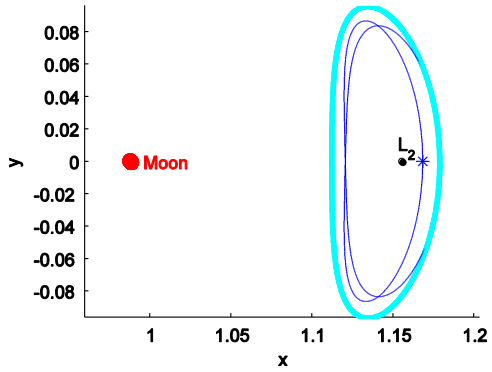

Figure 12 Solar sail Halo orbits at L_2 with *constrained* Earth-Moon line steering law. The thick cyan orbit is the natural Halo orbit in Figure 4a. a-b) Family of orbits. c) Orbit for $a_{0,EM} = 0.088$ (asterisk is initial condition).

IX. OUT-OF-PLANE SOLAR SAIL ACCELERATION

The steering laws proposed in Section V only consider an in-plane solar sail acceleration. However, the solar sail can be pitched with respect to the Earth-Moon plane to also create an out-of-plane acceleration component. This section will demonstrate the potential of this out-of-plane steering law by using the solar sail Lyapunov orbits at the L_1-point with a Sun-sail line steering law as a test case. Then, rather than adopting the in-plane law, $\hat{\mathbf{n}} = \hat{\mathbf{S}}$, the following out-of-plane Sun-sail line steering law is considered, see also Figure 15:

$$\mathbf{n} = \left[\cos\gamma\cos\left(\Omega_S t\right) \quad -\cos\gamma\sin\left(\Omega_S t\right) \quad \sin\gamma\right]^T \quad (12)$$

Note that for a pitch angle γ = 0, Eq. (12) reduces to the in-plane steering law.

a)

b)

c)

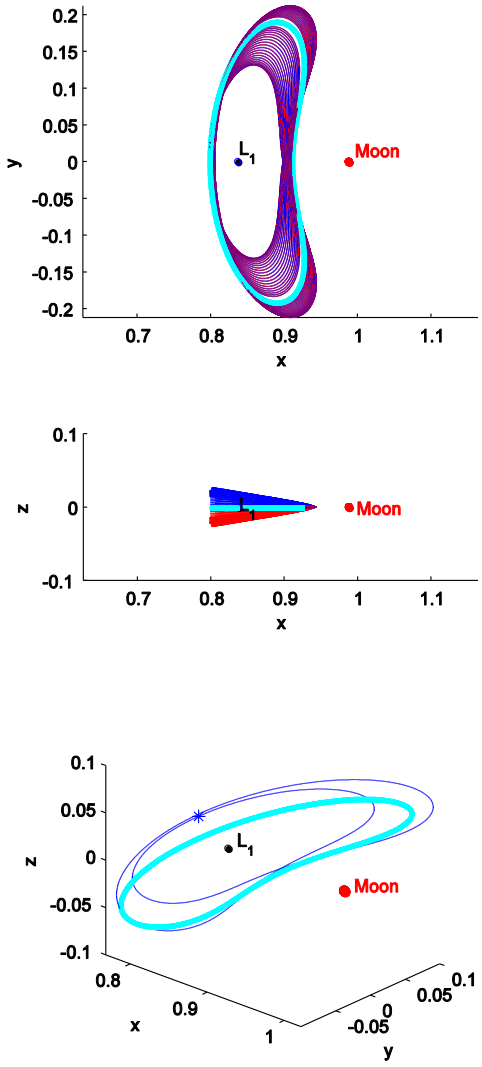

Figure 13 Solar sail Lyapunov orbits at L_1 with out-of-plane Sun-sail line steering law and $a_{0,EM}$ = 0.088. Orbits in blue and red are for $\gamma > 0$ and $\gamma < 0$, respectively. The thick cyan orbit is the natural Halo orbit in Figure 4. a-b) Family of orbits projected on the (*x*,*y*)- and (*x*,*z*)-planes. c) Orbit with maximum out-of-plane displacement (γ = 34.5 deg) (asterisk is initial condition).

To generate the family of out-of-plane Sun-sail line Lyapunov orbits at L_1, a continuation in γ is applied: starting from the planar solar sail Lyapunov orbit with γ = 0 and $a_{0,EM}$ = 0.088 in Figure 6b, the value for the pitch angle is slowly increased, the BVP is solved and the result is used as an initial guess for a slightly larger value for γ. The family of orbits that results from this is provided in Figure 13a-b for a range of pitch angles, $\gamma = [-60, 60]$ in deg. Note that the orbits for negative and positive values for the pitch angles are the same, only mirrored in the (x, y)-plane, and create out-of-plane displacements above en below the (x, y)-plane, respectively. The maximum out-of-plane displacement that is achieved in each orbit of the family is provided in Figure 14, which clearly shows that for a pitch angle of γ = 34.5 deg, the orbit extends farthest above or below the Earth-Moon plane. The corresponding orbit is depicted in Figure 13c and reaches an out-of-plane displacement of approximately 10,250 km.

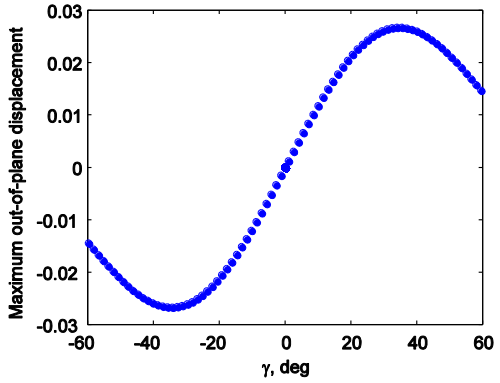

Figure 14 Maximum out-of-plane displacement in each orbit of the family of solar sail Lyapunov orbits at L_1 with out-of-plane Sun-sail line steering law (Figure 13) as a function of the solar sail pitch angle, γ.

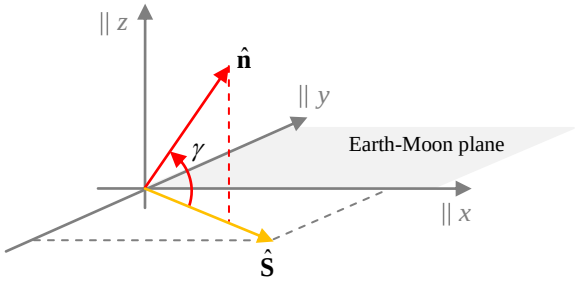

Figure 15 Schematic of out-of-plane Sun-sail line steering law

X. INITIAL CONDITION AT TIME t = 0

As indicated in Section II, the position of the Sun at time $t = 0$ is assumed to be on the negative x-axis. The actual Sun-sail configuration throughout the orbit and during one synodic lunar month then depends on the choice for the initial condition along the natural Halo orbit from where the continuation for solar sail periodic orbits starts. The choice for this initial condition will

influence the shape of the families of solar sail periodic orbits, which is demonstrated in this section by investigating different initial conditions for the solar sail Halo orbits with a constrained Earth-Moon line steering law, see Section VIII. As mentioned in Section VII, the results of Section VII.I are obtained by choosing the initial condition to be the y-axis crossing on the far-side of the L_2-point, i.e. below the Earth-Moon plane. As alternative, this section considers the y-axis crossing on the Earth/Moon-side of the L_2-point, i.e. above the Earth-Moon plane. When doing so, the result in Figure 16 is obtained.

Comparing Figure 12 and Figure 16 immediately shows the effect of the choice for the initial condition: when choosing the Earth-side y-axis crossing as initial condition, the solar sail Halo orbits increase in size compared to the natural Halo orbit, while for choosing the far-side y-axis crossing as initial condition, the solar sail Halo orbits decrease in size. This implies that very strict insertion constraints need to be imposed in order for the solar sail to enter the desired orbit.

Note that the effect on the out-of-plane motion is very similar for both initial conditions, i.e. the Halo orbits eventually reduce to planar Lyapunov orbits.

CONCLUSIONS

This paper has demonstrated the existence of solar sail periodic orbits in the non-autonomous Earth-Moon system. By solving the accompanying two-point boundary value problem and using a continuation approach, entire families of solar sail L_1-Lyapunov and L_2-Halo orbits have been found for increasing solar sail performances. Due to the non-autonomous behaviour of the system, all orbits have a period of one synodic lunar month and make two revolutions per orbital period. In addition, different families have been obtained for different in-plane solar sail steering laws: either keeping the solar sail perpendicular to the Earth-Moon line or to the Sun-sail line. As the latter can continuously exploit the maximum achievable solar sail acceleration, the families with a Sun-sail line steering law show a greater difference with respect to the natural Lyapunov or Halo orbits from which they bifurcate than the Earth-Moon line steering law. For both laws, the in-plane motion of the solar sail periodic orbits winds around the natural Lyapunov/Halo orbit, while for the Halo orbits the solar sail causes an off-set in the out-of-plane motion towards the Moon. When increasing the solar sail performance far enough, the Halo orbits even reduce to planar Lyapunov orbits. Furthermore, by introducing an out-of-plane steering law, the family of solar sail Lyapunov orbits at L_1 could be extended in the out-of-plane direction, achieving the maximum displacement for a sail pitch angle of 34.5 deg. Finally, the effect of different initial conditions, i.e. different initial Sun-sail configurations, have been investigated, showing a significant effect on the solar sail Halo orbits at L_2. This implies that insertion conditions are very strict in order to ensure that the desired solar sail Halo orbit is achieved.

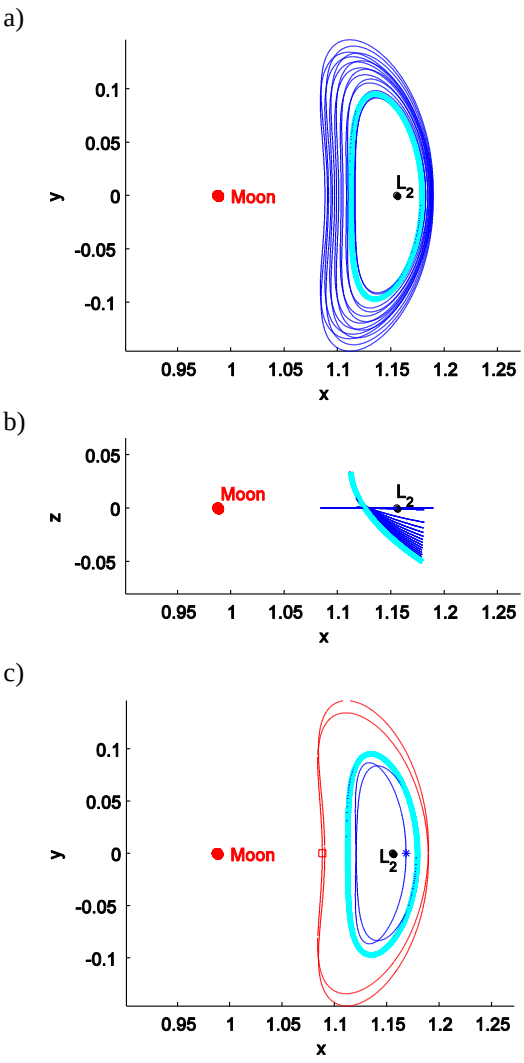

Figure 16 Effect of choice for initial condition at time $t = 0$ on the solar sail Halo family at L_2 for an Earth-Moon line steering law and for $a_{0,EM} = 0.088$. The blue solid line is the solar sail Halo orbit for $\mathbf{r}_0$ coinciding with the y-axis crossing on the far-side of the L_2-point (blue asterisk), the red dashed line is the solar sail Halo orbit for $\mathbf{r}_0$ coinciding with the y-axis crossing on the Earth/Moon-side of the L_2-point.

ACKNOWLEDGEMENTS

This work was funded by the European Research Council Advanced Investigator Grant-227571: Visionary Space Systems: Orbital Dynamics at Extremes of Spacecraft Length-Scale.

REFERENCES

1. Tsuda, Y., Mori, O., Funase, R., Sawada, H., Yamamoto, T., Saiki, T., Endo, T., Yonekura, K., Hoshino, H., and Kawahuchi, J. "Achievement of IKAROS - Japanese deep space solar sail demonstration mission," *Acta Astronautica* Vol. 82, 2013, pp. 183-188. doi: 10.1016/j.actaastro.2012.03.032
2. Johnson, L., Whorton, M., Heaton, A., Pinson, R., Laue, G., and Adams, C. "NanoSail-D: A Solar Sail Demonstration Mission," *Acta Astronautica* Vol. 68, 2011, pp. 571-575. doi: 10.1016/j.actaastro.2010.02.008
3. Braafladt, A. C., Artusio-Glimpse, A. B., and Heaton, A. F. "Validation of Solar Sail Simulations for the NASA Solar Sail Demonstration Project," *AIAA SPACE 2014 Conference and Exposition*. San Diego, CA, 2014.
4. Biddy, C., and Svitek, T. "LightSail-1 Solar Sail Design and Qualification," *Proceedings of the 41st Aerospace Mechanisms Symposium*. Pasadena, CA, 2012.
5. McNutt, L., Johnson, L., Clardy, D., Castillo-Rogez, J., Frick, A., and Jones, L. "Near-Earth Asteroid Scout," *AIAA SPACE 2014 Conference and Exposition*. American Institute of Aeronautics and Astronautics, San Diego, CA, 2014.
6. McInnes, C. R. *Solar Sailing: Technology, Dynamics and Mission Applications*. Berlin: Springer-Praxis Books in Astronautical Engineering, Springer-Verlag, 1999.
7. Goldstein, B. E., Buffington, A., Cummings, A. C., Fisher, R., Jackson, B. V., Liewer, P. C., Mewaldt, R. A., and Neugebauer, M. "A Solar Polar Sail Mission: Report of a Study to Put a Scientific Spacecraft in a Circular Polar Orbit About the Sun," *SPIE International Symposium on Optical Science, Engineering and Instrumentation*, 1998.
8. Heiligers, J., and McInnes, C. "Novel Solar Sail Mission Concepts for Space Weather Forecasting," *24th AAS/AIAA Space Flight Mechanics Meeting*. Santa Fe, NM, 2014.
9. Waters, T. J., and McInnes, C. R. "Periodic Orbits Above the Ecliptic in the Solar-Sail Restricted Three-Body Problem," *Journal of Guidance, Control, and Dynamics* Vol. 30, No. 3, 2007, pp. 687-693. doi: 10.2514/1.26232
10. McInnes, C. R., McDonald, A. J., Simmons, J. F. L., and MacDonald, E. W. "Solar Sail Parking in Restricted Three-Body Systems," *Journal of Guidance, Control, and Dynamics* Vol. 17, No. 2, 1994, pp. 399-406. doi: 10.2514/3.21211
11. McInnes, C. R. "Solar Sail Trajectories at the Lunar L2 Lagrange Point," *Journal of Spacecraft and Rockets* Vol. 30, No. 6, 1993, pp. 782-784. doi: 10.2514/3.26393
12. Simo, J., and McInnes, C. R. "Solar Sail Orbits at the Earth-Moon Libration Points," *Communications in Nonlinear Science and Numerical Simulation* Vol. 14, No. 12, 2009, pp. 4191-4196. doi: 10.1016/j.cnsns.2009.03.032
13. Wawrzyniak, G. G., and Howell, K. C. "Generating Solar Sail Trajectories in the Earth-Moon System Using Augmented Finite-Difference Methods (Article ID 476197)," *International Journal of Aerospace Engineering*, 2011. doi: 10.1155/2011/476197
14. Heiligers, J., Diedrich, B., Derbes, B., and McInnes, C. R. "Sunjammer: Preliminary End-to-End Mission Design," *2014 AIAA/AAS Astrodynamics Specialist Conference*. San Diego, CA, USA, 2014.
15. Howell, K. C. "Three-Dimensional, Periodic, 'Halo' Orbits," *Celestial Mechanics and Dynamical Astronomy* Vol. 32, 1983, pp. 53-71. doi: 10.1007/BF01358403